Theoretical studies on the control of oxidative phosphorylation in muscle mitochondria: application to mitochondrial deficiencies

Bernard KORZENIEWSKI*†‡ and Jean-Pierre MAZAT*

*Universite Bordeaux II, 146, rue Leo Saignat, F-33076 Bordeaux-Cedex, France, and †Institute of Molecular Biology, Jagiellonian University, al. Mickiewicza 3, 31-120 Kraków, Poland

1. The dynamic model of oxidative phosphorylation developed previously for rat liver mitochondria incubated with succinate was adapted for muscle mitochondria respiring on pyruvate. We introduced the following changes considering: (1) a higher external ATP/ADP ratio and an ATP/ADP carrier less displaced from equilibrium; (2) a substrate dehydrogenation more sensitive to the NADH/NAD^+ ratio; and (3) the respiratory chain, ATP synthase and phosphate carrier being more displaced from equilibrium. The experimental flux control coefficients already determined in state 3 for respiratory rate and ATP synthesis were used to adjust some parameters. This new oxidative phosphorylation model enabled us to simulate the whole titration curves obtained experimentally in state 3. These curves, which mimic the effect of mitochondrial complex deficiencies on oxidative phosphorylation, show a threshold effect, which is reproduced by the model. 2. The model was also used to simulate other physiological conditions such as: (i) state 3.5, conditions in-between state 4 and state 3; and (ii) hypoxic conditions. In both cases a profound change in the pattern of the control coefficients was shown. 3. This model was thus found useful in investigating a variety of new conditions, the most interesting of which can then be experimentally studied.

INTRODUCTION

The dynamic model of oxidative phosphorylation in liver mitochondria and intact hepatocytes developed previously [1–4] proved to be able to mimic the pattern of the system behaviour for a broad range of conditions and properties, as well as to predict the results of new experiments [5]. It was also helpful to explain the mechanisms underlying the macroscopic properties of oxidative phosphorylation, allowing a deeper insight into the control and regulation of this process. Finally, the model was used to study some new properties of the system which are difficult to predict in an intuitive way [6,7].

However, the model quantitatively described liver mitochondria only. It is well known that mitochondria from other tissues (especially skeletal muscle and heart) exhibit somewhat different properties. These involve the values of the respiratory control ratio (RCR), flux control coefficients for particular components of oxidative phosphorylation, and relative concentrations of complexes and carriers. Skeletal muscle is a very interesting tissue from the bioenergetic point of view, because changes in energy demand (followed by changes in the respiration rate) are much greater there than in the liver. Therefore more efficient controlling and regulating mechanisms of ATP synthesis are necessary. Muscle is a tissue with a high energetic requirement, and thus is particularly sensitive to deficiencies of oxidative phosphorylation complexes leading to mitochondrial myopathies [8–13]. Therefore, to deal with such problems in a theoretical way, it is necessary to modify the model of oxidative phosphorylation in liver in order to take into account the specific properties of muscle mitochondria.

A very useful set of experimental data, which could serve as a reference for the development of the model of oxidative phosphorylation in muscle mitochondria, appeared when flux control coefficients of particular steps of this process over respiration and ATP synthesis in state 3 were measured [14,15]. They have been used to adjust some parameters of the model. Furthermore, the titration curves of particular enzymes (or carriers) with specific inhibitors, performed for the calculation of the values of flux control coefficients, tell us not only about the system properties in the near vicinity of the original steady state (characterized by these coefficients), but also about the response of the system to large changes in complex activities, exhibiting in most of the cases a threshold effect already discussed in this context [16]. Such data are strictly relevant to the case of enzyme deficiencies.

Then the model was used in two ways. First to compare the simulated titration curves of respiration in state 3 by individual step activity (which mimic complex deficiency) with our experimental data determined in the presence of specific inhibitors; secondly, to simulate other physiological conditions: i.e. (i) an intermediate state between state 4 and state 3 (state 3.5), and (ii) hypoxic conditions. In these two latter cases, the control pattern of oxidative phosphorylation was shown to be profoundly changed.

It should be noticed that this model fits our results on rat quadriceps muscle mitochondria. It is known that the extent of oxidative phosphorylation is slightly different from one type of muscle to another, depending on the relative proportion of type I (oxidative) or type II (glycolytic) fibres. Thus our model should be adapted if different kinds of muscle are considered.

MODEL

The detailed description of the model, developed for oxidative phosphorylation in liver, is given elsewhere [1–4]. We will only

‡ To whom correspondence should be addressed at: Institute of Molecular Biology, Jagiellonian University, al. Mickiewicza 3, 31-120 Kraków, Poland.

Table 1 Set of chosen kinetic parameters and variables used in the model

Parameter description	Term
Michaelis–Menten constant of substrate dehydrogenation for the $NAD^+/NADH$ ratio	$K_{mN} = 100$
Real (not apparent) Michaelis–Menten constant of cytochrome oxidase for oxygen	$K_{mO} = 120\ \mu M$
Michaelis–Menten constant of hexokinase for ATP	$K_{mA} = 150\ \mu M$
'Half-saturation' constants of complexes I and III for their thermodynamic spans	$K_{mC1} = 2.5$ mV, $K_{mC3} = 2.1$ mV
Thermodynamic spans of complexes I and III	ΔE_{C1}, ΔE_{C3}
Thermodynamic span of the reaction catalysed by the ATP synthase and ATP/ADP carrier	ΔG_{SN}, ΔG_{EX}
Concentration of the reduced form of cytochromes a_3 and cytochrome c	a^{2+}, c^{2+}
Relative 'sensitivity coefficient' of substrate dehydrogenation to the $NAD^+/NADH$ ratio	$p_D = 0.6$
Constants used in a phenomenological kinetic description of proton leak	k_{LK1}, k_{LK2}, k_{LK3}

Table 2 Kinetic descriptions of the components of oxidative phosphorylation taken into account explicitly in the model

Description	Term
Substrate dehydrogenation:	$v_{DH} = k_{DH}\dfrac{1}{\left(1+\dfrac{K_{mN}}{NAD^+/NADH}\right)}p_D$
Complex I:	$v_{C1} = k_{C1}\dfrac{1}{1+\dfrac{K_{mC1}}{\Delta E_{C1}}}$
Complex III:	$v_{C3} = k_{C3}\dfrac{1}{1+\dfrac{K_{mC3}}{\Delta E_{C3}}}$
Complex IV:	$v_{C4} = k_{C4}\cdot a^{2+}\cdot c^{2+}\dfrac{1}{1+\dfrac{K_{mO}}{O_2}}$
ATP synthase:	$v_{SN} = k_{SN}\dfrac{\gamma-1}{\gamma+1},\quad \gamma = 10^{\Delta G_{SN}F/Z}$
ATP/ADP carrier:	$v_{EX} = k_{EX}\cdot\left(\dfrac{ADP_{fe}}{ADP_{fe}+ATP_{fe}\cdot 10^{-\Psi_e/Z}}-\dfrac{ADP_{fi}}{ADP_{fi}+ATP_{fi}\cdot 10^{-\Psi_i/Z}}\right)\cdot 10^{\Delta G_{EX}F/Z\,0.3}$
Phosphate carrier:	$v_{Pi} = k_{Pi}\cdot(Pi_e\cdot H_e - Pi_i\cdot H_i)$
ATP usage (hexokinase):	$v_{UT} = k_{UT}\dfrac{1}{1+\dfrac{K_{mA}}{ATP_{fe}}}$
Proton leak:	$v_{LK} = k_{LK1}\cdot(10^{k_{LK2}\Delta\Psi}-1)+k_{LK3}\cdot\Delta p$

mention here the modifications introduced during the extension of this model to muscle mitochondria. All other parameter values and kinetic descriptions are assumed to be the same as in liver mitochondria.

Only a few changes were introduced into our original model. Intending to model oxidative phosphorylation in mitochondria respiring on a physiological substrate, e.g. pyruvate, we used the general kinetic description of the substrate dehydrogenation subsystem applied earlier for intact hepatocytes [3]. This simple phenomenological expression describes the whole tricarboxylic acid cycle as well as the system of metabolite transport through the inner mitochondrial membrane:

$$v_{DH} = k_{DH}\frac{1}{\left(1+\dfrac{K_{mN}}{NAD^+/NADH}\right)}p_D \tag{1}$$

where $K_{mN} = 100$ is the Michaelis–Menten constant for the $NAD^+/NADH$ ratio and $p_D = 0.6$ reflects the sensitivity of substrate dehydrogenation to this ratio. The value of p_D is higher here than in liver and reflects a greater sensitivity of substrate dehydrogenation to NADH supply in muscle. A greater sensitivity towards $NAD^+/NADH$ ratio can be deduced from the low control coefficient of this step in state 3 [5].

The respiratory chain (apart from cytochrome oxidase) in liver mitochondria was described as working near equilibrium. In such a case, a near-linear dependence on the thermodynamic span through a considered reaction could be used. However, when the reaction goes further away from equilibrium (which is probably the case for the respiratory chain in muscle, at least near state 3), it gradually becomes saturated with its thermodynamic force [17] and the rate of this reaction cannot be increased any further. This property is reflected in the following hyperbolic kinetic descriptions of complex I and complex III activity, used in this paper:

$$v_{C1} = k_{C1}\frac{1}{1+\dfrac{K_{mC1}}{\Delta E_{C1}}} \tag{2}$$

and

$$v_{C3} = k_{C3}\frac{1}{1+\dfrac{K_{mC3}}{\Delta E_{C3}}} \tag{3}$$

where $K_{mC1} = 2.5$ mV and $K_{mC3} = 2.1$ mV are 'half-saturation' constants, while ΔE_{C1} and ΔE_{C3} denote thermodynamic spans of complex I and III, respectively. The relevant variables in these equations are the ratios $K_{mC1}/\Delta E_{C1}$ and $K_{mC3}/\Delta E_{C3}$. The value of ΔE_{C1} and ΔE_{C3} are arbitrarily set to 1 mV in state 3.5 and the values of K_{mC1} and K_{mC3} are adjusted to fit the known pattern of control coefficients assessed in state 3 (see below and [5]). State 3.5, between state 4 and state 3, denotes the 'physiological' initial steady state and corresponds to a respiratory rate representing 40 % of the maximal rate. The initial levels of reduction of cytochrome c, ubiquinone and NAD were calculated on the basis of initial ΔE_{C1} and ΔE_{C3} values.

The external ATP/ADP ratio was assumed to be equal to 150

in state 3.5 [18,19], compared with the value of 24 in liver [3,4], while the internal ATP/ADP ratio as well as the proton motive force were kept almost the same as in liver (3.2 and 180 mV respectively). This implies that the displacement of the ATP/ADP carrier from equilibrium was about six times less in muscle than in liver. This property could reflect the much higher relative concentration of the ATP/ADP carrier in muscle, when compared with the concentration of the ATP synthase or phosphate carrier. Accordingly, the two latter values should be slightly more displaced from equilibrium in muscle. In comparison with liver, we increased the displacement from equilibrium of the ATP synthase and of the phosphate carrier in the initial point (state 3.5). The new values for displacement from equilibrium, 1.4 for ATP synthase (instead of 1.1 in liver) and 1.2 for phosphate carrier (instead of 1.1 in liver), were chosen to fit the pattern of control coefficients in state 3. The concentrations of internal ATP, ADP and P_i were calculated from the assumed displacements from equilibrium of the ATP synthase and phosphate carrier (in the initial steady state 3.5).

The rate expressions for all the enzymes (processes) taken into account explicitly in the model are presented in Table 2. The notations are the same as in [1–4], where the complete definitions are given.

In order to achieve state 3, the rate constant of ATP utilization is increased 10 times compared with the rate constant in state 3.5, which corresponds experimentally to a 10-fold increase in the hexokinase concentration in a system of glucose–hexokinase used to simulate the energy load of the cell.

The flux control coefficient of a given step is calculated by varying the rate constant of this step by 0.1 % ($\Delta v/v = 0.001$). After a new steady state has been reached the relative variation of the flux $\Delta J/J$ is calculated and divided by the relative variation of the step activity in order to obtain the flux control coefficient: $C = (\Delta J/J)/(\Delta v/v)$.

THEORETICAL RESULTS AND DISCUSSION

The model gives a decrease in Δp of about 26 mV during state 4 → state 3 transition, while the respiration rate increases approximately nine times, in accordance with the best respiratory control ratio obtained in our experimental conditions.

The calculated values of the flux control coefficients for different components of oxidative phosphorylation over oxygen consumption in state 4, state 3 and in the intermediate state called state 3.5, as well as over ATP synthesis in state 3 are presented in Table 3 and Figure 1. State 3 and state 3.5 were reached by increasing the rate constant for the ATP usage (corresponding to the addition of increasing concentrations of hexokinase in the presence of glucose). The values for state 3 (data for other states in muscle mitochondria are not available in the literature) agree well, both for the respiration and ATP synthesis fluxes, with the values obtained experimentally [14,15]. The pattern of control of both fluxes is very similar in state 3, because the proton leak is insignificant under these conditions, and the oxygen consumption changes in parallel with ATP synthesis. In state 3, the control is shared more or less uniformly between many steps, namely complex III (the main controlling factor), complex I, ATP/ADP carrier, ATP synthase, phosphate carrier, substrate dehydrogenation and cytochrome oxidase. This is unlike what occurs in liver mitochondria incubated with succinate, where most of the control in state 3 is kept by the ATP/ADP carrier and dicarboxylate carrier [20,21]. In muscle

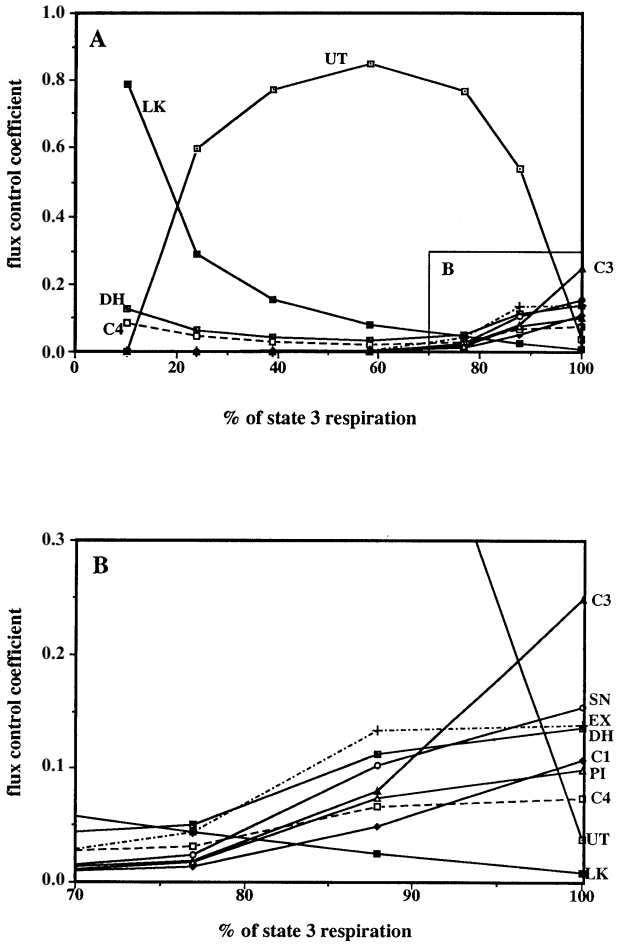

Figure 1 Simulated flux control coefficients for different enzymes or complexes of oxidative phosphorylation in muscle mitochondria in state 4, state 3 and the intermediate state (state 3.5)

(**A**) Abbreviations: UT, ATP utilization; LK, proton leak; C1, complex I; C3, complex III; C4, complex IV (cytochrome oxidase); DH, substrate dehydrogenation; SN, ATP synthase; EX, ATP/ADP carrier; PI, phosphate carrier. (**B**) An enlarged fragment of (**A**) in the vicinity of state 3.

Table 3 Simulated flux control coefficients for different components of oxidative phosphorylation in muscle mitochondria over the respiration flux in state 4, state 3.5 and state 3 as well as over the ATP synthesis flux in state 3

The values given in bold numbers denote the highest flux control coefficients in each state.

	Flux control coefficient			
	Over respiration			Over ATP synthesis
Enzyme (process)	State 4	State 3.5	State 3	State 3
Substrate dehydrogenation	0.13	0.03	0.14	0.13
Complex I	0.00	0.00	0.11	0.10
Complex III	0.00	0.01	**0.26**	0.24
Complex IV	0.08	0.02	0.07	0.07
Proton leak	**0.79**	0.08	0.01	−0.01
ATP synthase	0.00	0.00	0.16	0.18
ATP/ADP carrier	0.00	0.00	0.14	0.16
Phosphate carrier	0.00	0.00	0.10	0.11
Hexokinase	0.00	**0.85**	0.04	0.04

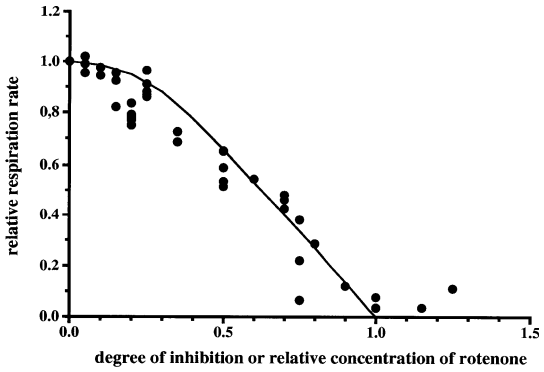

Figure 2 Experimental and simulated titration curves for complex I in state 3

The relative respiration rate is plotted against the degree of inhibition (simulated line) or the relative concentration of rotenone given in arbitrary units (experimental points). The relative rotenone concentration is calculated by dividing the actual rotenone concentration by the rotenone concentration giving the maximal inhibition of the flux.

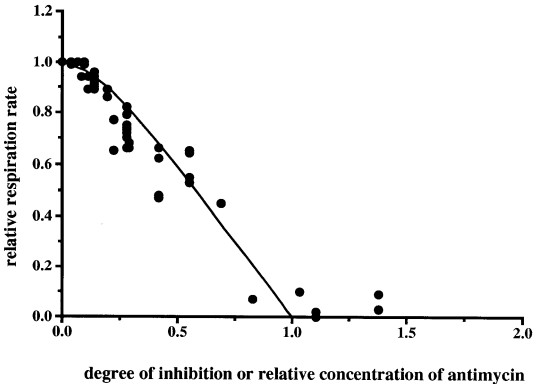

Figure 3 Experimental and simulated titration curves for complex III in state 3

The relative respiration rate is plotted against the degree of inhibition (simulated line) or the relative concentration of antimycin given in arbitrary units (experimental points). The relative antimycin concentration is calculated by dividing the actual antimycin concentration by the antimycin concentration giving the maximal inhibition of the flux.

mitochondria, with pyruvate as respiratory substrate, as compared with liver mitochondria incubated with succinate, some control is probably shifted from substrate dehydrogenation to the respiratory chain and from the ATP/ADP carrier to the ATP synthase and phosphate carrier.

In intermediate states [state 3.5 corresponds to about 40% of the maximal (state 3) respiration rate] the simulated pattern of control was quite different. The main controlling factor there was the ATP usage (hexokinase) which controlled up to 85% of the flux. The small remaining part of the control was mainly due to proton leakage. The maximal control exerted by hexokinase in muscle mitochondria (0.85) was significantly greater than in liver mitochondria (up to about 0.6) [20,21]. In state 4, as in liver mitochondria, most of the control was at proton leakage, with substrate dehydrogenation and cytochrome oxidase being responsible for the remainder.

It can be concluded that muscle mitochondria are more sensitive than liver mitochondria to changes in the energy demand of the cell, as is simulated by an increase in ATP consumption by

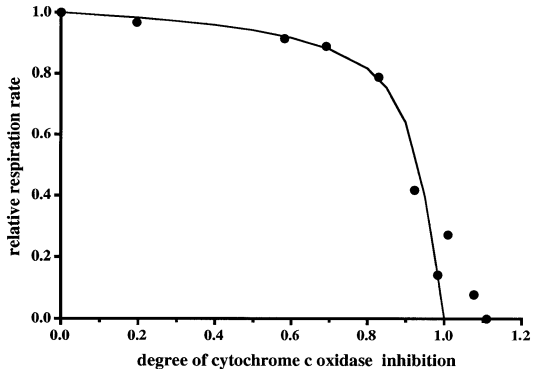

Figure 4 Experimental and simulated titration curves for complex IV (cytochrome *c* oxidase) in state 3

The simulated curve and the experimental points are both plotted against the degree of inhibition of cytochrome *c* oxidase activity.

hexokinase. Two criteria can be formulated to assess the relative sensitivity (elasticity) of mitochondria, as whole entities, to the external ATP/ADP ratio: the respiratory control ratio and the maximal flux control coefficient for hexokinase in state 3.5. The fact that we use hexokinase in both systems enables us to compare directly the responses of skeletal muscle and liver oxidative phosphorylation. The respiratory control ratio and the maximal flux control coefficient for hexokinase in state 3.5 are higher in muscle mitochondria. This result can be understood in considering the fact that skeletal muscle has to respond to greater fluctuations in energy demand than liver. However, the quantitative theoretical results obtained here cannot be directly extrapolated to intact myocytes, since the ATP-consuming system in cells probably has a more complex sensitivity to the external ATP/ADP ratio than hexokinase has.

In Figures 2–7 comparison is made between the simulated dependence of the respiration rate on the degree of inhibition of particular steps, and the titration curves for these steps obtained experimentally by addition of increasing amounts of specific inhibitors in state 3. Good agreement is found, of course, at low inhibitor concentrations, because the experimental control coefficient values were used to adjust some parameters of the model. But, in addition, the agreement can also be prolonged for higher inhibitor concentrations. This suggests that the general properties on which the model is built, are reasonable. The fit is less good around maximal inhibition because, for comparison of experimental points and theoretical curves, we supposed that the inhibition curve of the isolated step is linear. This is, in most of the cases, an approximation, only valid at the lower concentration of inhibitor. This is the reason why near maximal inhibition, the experimental points are no longer on the simulated curve: in this region, the degree of inhibition of the isolated step is no longer proportional to the concentration of the inhibitor. However, in the case of the complex IV titration curve, it is possible to assess simultaneously the effect of KCN on the respiratory flux and on the rate of isolated cytochrome *c* oxidase [16,22,23], so that, it is possible to represent the experimental rate of respiration as a function of the actual activity of the isolated step (Figure 4). It has to be stressed that the inhibitor titration curves, used for control coefficient determination, also mimic the response of oxidative phosphorylation towards respiratory complex deficiencies as they occur in mitochondrial pathologies. We would like

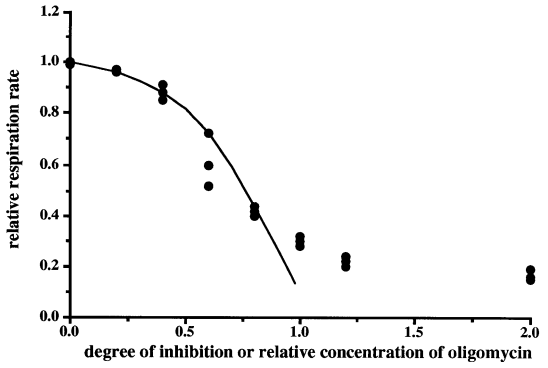

Figure 5 Experimental and simulated titration curves for ATP synthase in state 3

The relative respiration rate is plotted against the degree of inhibition (simulated line) or the relative concentration of oligomycin given in arbitrary units (experimental points). The relative oligomycin concentration is calculated by dividing the actual oligomycin concentration by the oligomycin concentration giving the maximal inhibition of the flux.

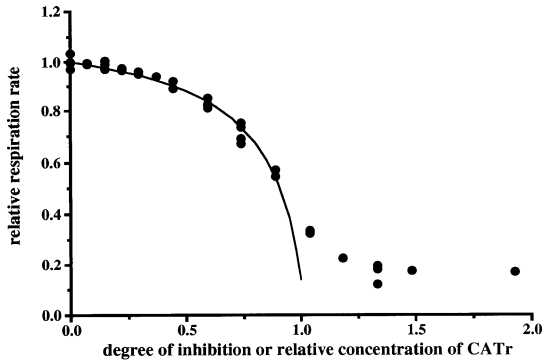

Figure 6 Experimental and simulated titration curves for ATP/ADP carrier in state 3

The relative respiration rate is plotted against the degree of inhibition (simulated line) or the relative concentration of carboxyatractylate (CATr) given in arbitrary units (experimental points). The relative CATr concentration is calculated by dividing the actual CATr concentration by the CATr concentration giving the maximal inhibition of the flux.

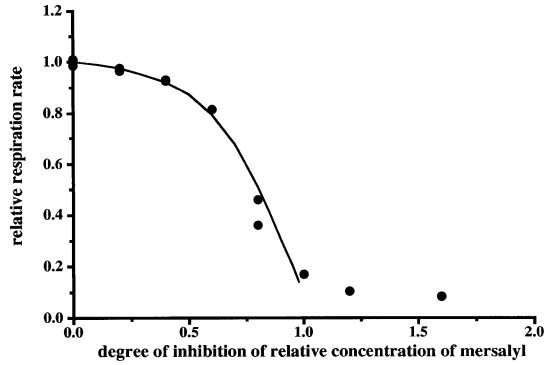

Figure 7 Experimental and simulated titration curves for phosphate carrier in state 3

The relative respiration rate is plotted against the degree of inhibition (simulated line) or the relative concentration of mersalyl given in arbitrary units (experimental points). The relative mersalyl concentration is calculated by dividing the actual mersalyl concentration by the mersalyl concentration giving the maximal inhibition of the flux.

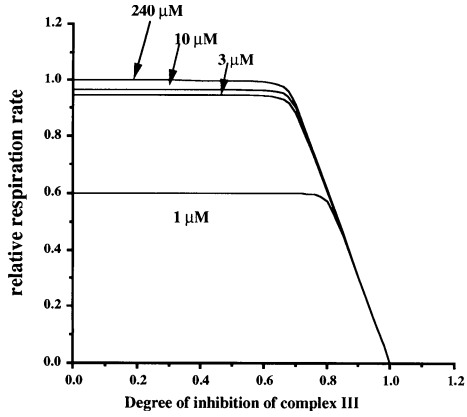

Figure 8 Simulated titration curve for complex III in state 3.5 ($vO_2 = 0.4 \times vO_2^{max}$) at different concentrations of oxygen as indicated on the Figure

to stress more particularly that most of these curves exhibit a threshold already discussed in [16] in the framework of metabolic control theory. This threshold effect can be described in the following way: the inhibition of the activity of a given complex has little effect on the flux (respiratory flux or ATP synthesis) until a rather high threshold value (70 % in the case of cytochrome *c* oxidase in Figure 4 for instance); above this value, an abrupt decrease of the flux is observed. This peculiar behaviour was not only observed in inhibition experiments [5–7], but also in patients' biopsies or in cell cultures [24–29] and appears as a characteristic salient feature of mitochondrial pathologies.

It must be pointed out that our model simulates the effect of an evenly distributed decrease in the activity of respiratory chain complexes. This is particularly the case with nuclear mutations equally affecting all the mitochondria of all tissues. In this case, although the extent of the deficiency is the same in all the tissues, some of them can be more affected by the defect than others because the threshold in the expression of the defect on the respiratory rate or on the mitochondrial ATP synthesis can be different. This difference in threshold can be undersood in relationship with the value of the control coefficients of the deficient step, which depends upon (i) the composition in mitochondria of the various complexes of the respiratory chain and mitochondrial ATP synthesis machinery, including tissue specificity of some subunits of the respiratory complexes; (ii) the steady state of oxidative phosphorylation functioning, which is different in different tissues in various physiological states; and (iii) the oxygenation of the tissue (see the discussion below, which can also be viewed as a particular reason for which the steady state of oxidative phosphorylation can be changed).

This type of evenly distributed defects in one complex has to be distinguished from the defects due to mutations in mitochondrial DNA. In this latter case, the heteroplasmy of mitochondrial DNA (the amount of mutated mitochondrial DNA in relation to total mitochondrial DNA) varies from one tissue to another and even from one cell to another in the same tissue, giving rise to a mosaic aspect of muscle fibres in this case when they are stained for the deficient complex (this is the case in cytochrome *c* oxidase deficiencies). The difference in the heteroplasmy in different tissues can, in this case, explain the tissue specificity of some complex deficiencies.

Our model, assuming implicitly that all mitochondria are similar, does not apply to this more complex case. In this latter case, the expression of complex deficiencies and, more par-

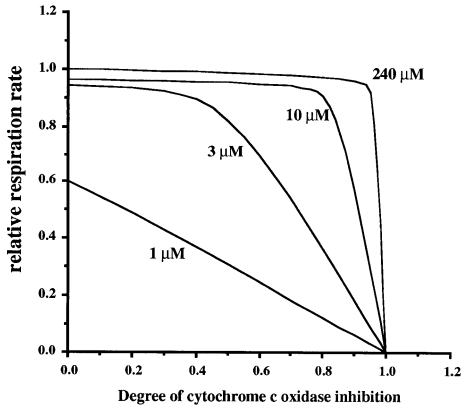

Figure 9 Simulated titration curve for complex IV (cytochrome oxidase) in state 3.5 ($vO_2 = 0.4 \times vO_2^{max}$) at different concentrations of oxygen as indicated in the Figure

ticularly, the existence of a tissue-specific threshold for this expression, have to take into account not only the extent of the defect itself, but also the distribution of the defect (i.e. the distribution of mitochondrial DNA heteroplasmy) in the tissue, or in the cell or even in the individual mitochondria. These points will be investigated in future studies.

The fact that our model gives a reasonably fit of our experimental data in state 3 prompted us to apply it to other, perhaps more physiological conditions. Mitochondria in intact cells are probably never exactly in state 3 but in a state comparable, more or less, to state 3.5. After muscle contraction, this state is, of course, shifted by calcium towards much greater values of the respiration rate; nevertheless, the change in ATP/ADP ratio under these conditions is probably much less than the change in ATP/ADP ratio in the transition from state 3.5 to state 3, because of the concomitant activation of different steps [30]. For this reason, state 3.5 of isolated mitochondria seems to be more relevant to the conditions occurring in intact cells than does state 3. We derived the control coefficient pattern of respiratory flux in these conditions (Table 3). We have mentioned earlier that a completely different control pattern is obtained. The inhibitor titration curves were also quite different. Two examples (for complex III and IV) are given in Figures 8 and 9. Generally, the inhibitor titration curves in state 3.5 exhibit a large plateau region which remains until the given step has been inhibited by at least 60%. Then, a steep threshold can be observed, in correlation with the very low flux control coefficients calculated under these conditions.

Hypoxia was the other condition explored in this study, because it is relevant during muscle exercise and it is well known that some mitochondrial deficiencies can only be diagnosed in this way. Figures 8 and 9 shows the simulated effect of decreasing oxygen concentration on complexes III and IV titration by their corresponding inhibitors respectively. Comparing these two Figures, it is clear that complex III never controls oxidative phosphorylation whatever the oxygen concentration is. It clearly appears, however, that the control coefficient of cytochrome *c* oxidase does not change until 3 μM, but that the threshold value decreases much more than in Figure 8 (around 95% at 240 μM and 40% at 3 μM). When oxygen concentration decreases to 1 μM, which is around the apparent K_m value of cytochrome *c* oxidase for oxygen, this complex becomes completely controlling. This Figure reveals a role that can be played, either through the threshold value or more directly through its control, by a deficiency in this complex at lower (and more physiological) concentrations of oxygen in tissues.

To sum up, we have adapted to skeletal muscle mitochondria a model of oxidative phosphorylation previously developed for liver mitochondria. This model fits our experimental results obtained in state 3 conditions well. It also allows us to predict that profound changes in the control coefficient panel of oxidative phosphorylation can be expected in other physiological or pathological conditions. These new conditions will now be explored experimentally.

We are grateful to Vida Mildaziene and Thierry Letellier for stimulating discussions. This work was supported by the Association Française contre les Myopathies (A.F.M), the Université Bordeaux II and the Région Aquitaine. We wish to thank M. N. Grangeon for correcting the English.

REFERENCES

1 Korzeniewski, B. and Froncisz, W. (1991) Biochim. Biophys. Acta **1060**, 210–223
2 Korzeniewski, B. and Froncisz, W. (1992) Biochim. Biophys. Acta **1102**, 67–75
3 Korzeniewski, B. (1996) Biophys. Chem. **58**, 215–224
4 Korzeniewski, B. (1996) Biophys. Chem. **57**, 143–153
5 Korzeniewski, B., Harper, M.-E. and Brand, M. (1995) Biochim. Biophys. Acta **1229**, 315–322
6 Korzeniewski, B. and Froncisz, W. (1993) in Modern Trends in BioThermoKinetics (Schuster, S., Rigoulet, M., Ouhabi, R. and Mazat, J.-P., eds.), pp. 33–38, Plenum Press, New York
7 Korzeniewski, B. (1996) Biophys. Chem. **59**, 75–86
8 Morgan-Hughes, J. A. (1986) in Myology (Engel, A. G. and Banker, B., eds.), McGraw Hill
9 Di Mauro, S., Bonilla, E., Zeviani, M., Walton, J. and de Vivo, D. C. (1985) Ann. Neurol. **17**, 521–538
10 Wallace, D. C. (1992) Annu. Rev. Biochem. **61**, 1175–1212
11 Wallace, D. C. (1993) Trends Genet. **9**, 128–133
12 Lestienne, P. (1989) Biochimie **71**, 1115–1123
13 Holt, I. J., Miller, D. H. and Harding, A. E. (1989) J. Med. Genet. **26**, 739–743
14 Letellier, T., Malgat, M. and Mazat, J.-P. (1993) Biochim. Biophys. Acta **1141**, 58–64
15 Jouaville, L., Ichas, F., Letellier, T., Malgat, M. and Mazat, J.-P. (1993) in Modern Trends in BioThermoKinetics (Schuster, S., Rigoulet, M., Ouhabi, R. and Mazat, J.-P., eds.), pp. 319–325, Plenum Press, New York
16 Letellier, T., Heinrich, R., Malgat, M. and Mazat, J.-P. (1994) Biochem. J. **302**, 171–174
17 Westerhoff, H. V. and van Dam, K. (1987) Thermodynamics and Control of Biological Free-Energy Transduction, Elsevier, Amsterdam
18 Funk, C. J., Clark, A. and Connet, R. J. (1990) Am. J. Physiol. **258**, C995–C1005
19 Meyer, R. A. and Foley, J. M. (1994) Med. Sci. Sports Exerc. **26**, 52–57
20 Groen, A. K., Wanders, R. J. A., Westerhoff, H. W., van der Meer, R. and Tager, J. M. (1982) J. Biol. Chem. **257**, 2754–2757
21 Gellerich, F. N., Bohnensack, R. and Kunz, W. (1983) Biochim. Biophys. Acta **722**, 381–391
22 Mazat, J.-P., Letellier, T., Malgat, M., Jouaville, S. and Morkuniene, R. (1994) in What is Controlling Life? (Gnaiger, E., Gellerich, F. N. and Wyss, M., eds.), pp. 272–274, Innsbruck University Press, Innsbruck
23 Gellerich, F. N., Kunz, W. and Bohnensack, R. (1990) FEBS Lett. **274**, 167–170
24 Wallace, D. C. (1986) Somatic Cell Mol. Genet. **12**, 41–49
25 Shoffner, J. M., Lott, M. T., Lezza, A. M. S., Seibel, P., Ballinger, S. W. and Wallace, D. C. (1990) Cell **61**, 931–937
26 Chomyn, A., Martinuzzi, A., Yoneda, M., Daga, A., Hurko, O., Johns, D., Lai, S. T., Nonaka, I., Angelini, C. and Attardi, G. (1992) Proc. Natl. Acad. Sci. U.S.A. **89**, 4221–4225
27 Hayashi, J. I., Ohta, S., Kikuchi, A., Takemitsu, M., Goto, Y. and Nonaka, I. (1991) Proc. Natl. Acad. Sci. U.S.A. **88**, 10614–10618
28 Sciacco, M., Bonilla, E., Schon, E. A., DiMauro, S. and Moraes, C. T. (1994) Human Mol. Genet. **3**, 13–19
29 Moraes, C. T., Ciacci, F., Bonilla, E., Ionasescu, V., Schon, E. A. and DiMauro, S. (1993) Nature Genet. **4**, 284–288
30 Hochachka, P. W. and Matheson, G. O. (1992) J. Appl. Physiol. **73**, 1697–1703

Received 7 February 1996/16 May 1996; accepted 12 June 1996